The miniature paleo-speleothems record of the 'greening' Earth in the early Ediacaran (635 Ma)

Guanghong Zhou[1,2,7], Tian Gan[3,4,7], Taiyi Luo[3*], Mingzhong Zhou[5], Weijun Luo[6], Shijie Wang[6]

[1] *School of Geography and Resources, Guizhou Education University, Guiyang 550018, China*

[2] *Guizhou Provincial Key Laboratory of Geographic State Monitoring of Watershed, Guizhou Education University, Guiyang 550018, China*

[3] *State Key Laboratory of Ore Deposit Geochemistry, Institute of Geochemistry, Chinese Academy of Sciences, Guiyang 550081, China*

[4] *University of Chinese Academy of Sciences, Beijing 101408, China*

[5] *School of Geographical and Environmental Sciences, Guizhou Normal University, Guiyang 550001, China*

[6] *State Key Laboratory of Environmental Geochemistry, Institute of Geochemistry, Chinese Academy of Sciences, Guiyang 550081, China*

[7]*co-first author*

*E-mail address: luotaiyi@vip.gyig.ac.cn

Abstract

A rapid transition from the snowball Earth to the 'greening' Earth in the early Ediacaran, triggered by enhanced terrestrial weathering and then by elevated primary productivity, has been speculated by isotope researches [3]. However, direct geological evidence of continental weathering in the early Ediacaran is still lacking. This study examines paleo-speleothems related to the karstic dissolution surface at the upmost cap dolostone of the early Ediacaran Doushantuo Formation (635 Ma). Observation of sheet-crack thin-sections from platform to slope facies in South China suggests that plentiful speleothem-like structures in chalcedony should be interpreted as low-temperature silicified calcareous paleo-speleothems. Furthermore, isopachous dolomite,

speleothems, chalcedony, and quartz should have filled sheet-cracks during the uplift, karstification, and subsequently hydrothermal processes before the secondary transgression. Thus these widely distributed paleo-speleothems, which are direct geological evidence for the ‘greening’ Earth in the early Ediacaran, might represent an initial formation of the soil-ecosystem after the barren snowball Earth.

1. Introduction

Paleo-climate evolution in the Neoproterozoic (1,000-542 Ma), the most notable of which was the abrupt climate transition in the aftermath of the Marinoan deglaciation (~635 Ma [4]) recorded in the 3-5 m cap dolostones and its idiosyncratic sedimentary structure, was the prelude to the Cambrian explosion. Isotopic studies [1-3] have described a rapid evolution from a snowball Earth to a 'greening' Earth, which could greatly enhance groundwater influx of photosynthetic carbon from phytomass and promote the 'clay mineral factory', and then subsequently increase the atmosphere’s O_2 content [5] and trigger the expansion of multicellular life. This rapid evolution centered on a drastic change of the continental weathering mode which elevated the bio-available P flux and promoted the marine primary productivity. Therefore, geological records of contemporaneous continental weathering are important clues to understanding the evolution of life in the Neoproterozoic and to illuminating the Cambrian explosion.

Karstification is the most important continental weathering process in carbonate distribution zones, of which the environment change could be record by speleothems (stalagmites, stalactites, flowstones etc.). Studies of modern karst caves suggest that speleothem deposition is mostly controlled by evolution of CO_2 contents in drip-water, which originate from precipitation (atmospheric CO_2) and supersaturation in soil zone (CO_2 from bio-respiration and organic decomposition) and then degassing in caves [6-8]. Thus paleo-speleothems in paleo-karst, such as dripstone [9], micro-stalactite [10,11] and stromatolitic laminae coatings [12], are significant evidence for subaerial exposure and paleo-pedogenesis. The widespread discontinuous karstic surface at the top of cap dolostones (635 Ma) in Africa, Canada and China has disclosed a global karstic dissolution event [13] caused by uplifting of continental shelf responding to deglacial isostatic rebound [14]. Hence, more detailed geological evidence such as paleo-speleothems are expected to be preserved in fissures, voids and sheet-cracks related to the karstic dissolution event [13].

In this paper, we report a series of miniature but delicate paleo-speleothems (including stalagmites, stalactites and coatings) preserved in the sheet-crack of Marinoan cap dolostone (~635 Ma) in South China. These paleo-speleothems further confirm the possibility of a broad and transient continental uplift with exposure and continental weathering due to the deglacial isostatic rebound.

2. Geological setting and observations

The Doushantuo Formation of basin, slope and platform facies is widely deposited on the Yangtze Block of South China (see Fig.1 in ref. [13]), and is underlain by Marinoan deglacial tillite unit. This shows a transition from purple diamicite (<100 m) in platform facies to grey diamicite (>1000 m) in basin facies. The 3-5 m cap dolostone in basal Doushantuo Formation from platform to slope facies is significant with disrupted massive dolomicrite and unique structures (such as giant wave ripples [15], teepee-like, sheet-cracks etc. [16]). A broadly karstic dissolution surface, caused by uplift by isostatic rebound, has been confirmed by geological observation in South China. The total duration (<1.0 Ma) from deposition to exposure and dissolution of the cap dolostone has been constrained by high-precision U-Pb zircon age of 634.57 ± 0.88 Ma at the topmost of Nantuo diamictite [4] and 635.23 ± 0.57 Ma at the topmost of cap dolostone [17,18], respectively. Remarkably, sheet-cracks have a uniform mineral paragenetic sequence across the entire Yangtze Block: they start with isopachous dolomites (sometimes with minor barite), followed by siliceous minerals (chalcedony and quartz), and ending with later stage calcite and barite [19].

Miniature but perfect stalactites and stalagmites, which are the most typical calcareous speleothems (gravitational dripping water forms) (Fig.1, Fig.2), have been gradually disclosed in chalcedony cements from thick (more than 2-3 cm) sheet-cracks of cap dolostones and distributing from slope (Wenghui and Daping) to platform facies (Xiaofenghe and Beidoushan) sections on the Yangtze Block. Based on this discovery, flat and thinner laminae, partly with botryoidal structures, that extensively encrust the ceiling and floor of the sheet-cracks or breccias (Fig.3), have been interpreted here as coatings (non-gravitational water-film forms).

2.1 stalactite

Many stalactites, hanging downwards from the ceiling of sheet-cracks and exhibiting as single one or conjoined by multi-stalactites, have been found in the Beidoushan and Wenghui sections (Fig. 1, 2a, 2e and 2d). The most common individual stalactites are elongated columns, ranging from less than 0.4 cm to about 1.0 cm in diameter, and from less than 1 cm to more than 3 cm in length.

Three growth stages could be identified by laminae rhythm in two vertical profiles of stalactites from the Beidoushan section (Fig.1). The first is the straight soda-straw with a central channel. The channel is about 100 μm in diameter and 1-2 cm in length and is lined by brown organisms and filled with cryptocrystalline chalcedony. The wall of the soda-straw is comprised of fibrous chalcedony with about 400-500 μm thickness and it is also coated by brown organisms. The second stage is distinguished by density rippling lamina couplets in flank and botryoid structures in the tip, which reflect stable and slow feeding. The final stage is composed of relative broader lamina couplets which reflect continuous and affluent feeding.

The cross-profiles of stalactites are distinguished by multilayer concentric circularity structures with alternations from dark to light. The significant difference, however, is the soda-straw structure, which is generally present in stalactites but absolutely absent in stalagmites. The three growth stages described above can be clearly observed in the cross-profiles of stalactites from the Beidoushan section. In the Wenghui section, however, only two growth stages are displayed in the cross-profiles of stalactites (Fig.2a, 2e and 2d) and in the vertical-profile of stalagmites. These differences suggest that the two sections have different paleo-enviornments.

2.2 stalagmite

Some stalagmites, which grow upwards from the floor of the sheet-crack, were discovered in Wenghui, Xiaofenghe and Beidoushan sections. They are mainly composed of translucent chalcedony, which makes them obviously distinguished from the surrounding white crystalline quartz in hand-specimens of the Wenghui and Beidoushan sections (Fig.2b, 2d and 2f). Most of them are cylindric in shape, slightly wider in the root and narrower in the tip, with length concentrated around 1-3.5 cm and diameters of about 0.5-1.3 cm. This thin diameter style, classified as "Minimum-diameter" stalagmite [20], is coincident with the short drip fall height [21] in the sheet-cracks.

A perfect vertical profile of stalagmite from the Wenghui section shows a clear transition of growth style (Fig.2b) under a reflecting light microscope, while, such a transition is relatively blurred under transmitted light. The early growth style is distinguished by a stacked botryoid structure, which could be observed in the bottom part of modern stalagmites [22-25] (Fig.2b) and which represent turbulence of the dripping water at the beginning of stalagmite deposition or indigent feeding and slow precipitation[26]. The later growth is significant with continuous and smooth rhythmical laminae couplets by a dark and a light lamina, which is similar to modern calcareous stalagmites [25,27,28] and which represent affluent feeding and stable precipitation [22,29-31]. The rhythmical laminae are about 350 μm thick and contain about 20-30 lamina couplets.

There is one complete stalagmite and three complete stalactite cross-profiles in the same slide, the latter of which are characterized by a central channel texture (Fig.2d). There are two growth stages. The first of these is typical of unity cryptocrystalline chalcedony and the latter of them is features concentric fibrous chalcedony laminae, corresponding to the two-growth style in the vertical profile as mentioned above (Fig.2b). There are about 20-30 laminae couplets within the 2100 μm thick outer zone and this is rich in organics as seen by the obvious increase in fluorescence (Fig.2c, 2e and 2f) when compared to the inner zone. Significantly, residue calcite core and laminae have been observed in one stalagmite cross-profile from the Xiaofenghe section (Fig.3h).

2.3 coatings

In almost all of the cap dolostone sections in South China, the wall (mainly composed of ceiling and floor) of the sheet-cracks and the breccias in them are extensively covered with less than 0.1 cm to 1 cm thick chalcedony coatings, which tend to have fairly continuous layers, and are characterized by visible rippled growth morphology and stacked layering (Fig. 3). Remarkably, partly silicified calcite coatings, which could be distinguished under reflected light and scanning electron microscope (SEM) (Fig.3e and 3f), was preserved in the Daping section. The coatings may be botryoidal (Fig. 3b), or even spiral (looks like vermiform helictites) (Fig.3c and 3d), but in most cases they are smoothly curving along the wall of the sheet-crack and the breccias with stable thickness (Fig. 3a). On the whole, the coatings comprise of 15-30 lamina couplets, which are much more obvious in ultraviolet fluorescent (Fig.2c and 3g), with single couplet thickness ranging from 20 μm to 60 μm. These morphology and laminae structure indicate that the smooth coatings periodically precipitated from adhesive water-films condensed from humid caves, the botryoidal structure are produced by surface tension dividing water-films into drops and the vermiform helictites produced by the addition of drip water to already present water-films.

3. Discussion

Protogenetic siliceous speleothems are commonly developed in caves or lava tunnels overlain by silicate rocks (such as quartzites, sandstones, granites etc.) [32]. Although platform-wide black shale overlaid on the cap dolostone [33] seems to be a potential silica source, lack of karstic surface and weathering dissolution textures in the black shale suggests that the sheet-crack speleothems were not protogenetic siliceous speleothems and were constrained before the deposition of the black shale. Indeed, the sheet-crack speleothems are confined below the widespread paleo-karstic surface the age of which has been previously determined by two ash beds with zircon U-Pb age of 634.57 ± 0.88 Ma and 635.23 ± 0.57 Ma [17,18] respectively. Additionally, the coatings in the Daping section are mostly consisted of calcareous laminae (Fig. 3e and 3f) and the silicified stalactites in Xiaofenghe section still retain a few calcareous laminae (Fig. 3h). Therefore, the sheet-crack speleothems deposited at ca. 635Ma were originally calcareous speleothems, which is akin to modern silicification-preserved speleothems formed by low-temperature metasomatism of primary calcareous speleothems [34,35].

Three successive events associated with the Marinoan cap dolostone in South China have been summarized as such [13]: (1) the first postglacial transgression and deposition of the cap dolostone; (2) isostatic rebound, uplift and karstification of the cap dolostone; and (3) the second postglacial transgression, multiphase cave fillings and post-cap deposition. Multiple mineral generations on walls of sheet-cracks are attributed to the beginning of the second postglacial transgression [13] or a low-temperature hydrothermal episode [19,36], however, minerals corresponding to the uplift and karstification event have not been depicted. No obvious dissolution phenomena by later erosion have been observed on the surface of the paleo-speleothems, indicating that the deposition of the paleo-speleothems has been quickly terminated by the low temperature hydrothermal process. Given that the hydrothermal episode developed after the beginning of the second transgression, chert lens (as siliceous tufa) should be observed upon the karstic surface, nevertheless, siliceous cements and veins have been strictly confined beneath the karstic surface. Thus we interpret the deposition and hydrothermal silicification of the sheet-crack calcareous speleothems as successive processes during exposure and karstification.

Modern karst studies indicate that necessary condition for karstic dissolution is the soil-ecosystem (soil, plant, microbial, etc.), which afford organic matter and plentiful CO_2 [37,38] in the water of an epikarst zone and hence the relative speleothems could partly record the overlying ecosystem information. Karst dissolution in some high-altitude and cold-climate regions occurs in the absence of soil [7], however, and so obviously a temperature gradient caused by a huge altitude drop is needed to form speleothems in these conditions. Paleo-karsts are defined as karsts developed largely or entirely during past geological periods [39]. Freytet (2002) refers to karsts or vugs that are centimeters to decimeters as microkarsts [11], and these are an important evidence of ancient subaerial exposure and paleosols formation [9,11,40]. Like pseudomicrokarsts [11], we define the microkarsts developed in past geological periods as paleomicrokarsts, in which the speleothems are defined as paleomicrospeleothems. The Precambrian palaeosols are habitats for early terrestrial life. The paleomicrospeleothems in the corresponding carbonate strata are important geological evidence that record the early biological evolution of the Earth. Paleomicrospeleothems (fibrous flowstone lining grike system) found in the Mesoproterozoic in Canada [41] and U.S.A [35] and the exquisite paleomicrospeleothems (icicle-like pendants, hemispherical protrusions and ground-up columns) reported in the Dengying Formation [42] may represent contemporaneous pedogenesis processes. In the early Ediacaran, although recovery of ocean-ecosystem from the brutal snowball Earth had been confirmed by vase-shaped fossils in tillite, the geological evidence for terrestrial-ecosystem revival are still expected yet. Here, the silicified paleomicrospeleothems preserved in the 3-5 m cap dolostone suggest that the soil-ecosystem had been broadly established in South China just after uplifting and exposing of the cap dolostone.

4. Summary and Implication

This paper reports the widely distributed miniature silicified paleospeleothems in sheet-cracks in Marinoan cap dolostone from South China, which depict specific karstic process of the cap dolostone during uplifting and exposure caused by isostatic rebound. These are 1) miniature speleothem growth during karstification; 2) speleothem termination and silicification by low-temperature fluid before the second transgression.

These paleo-speleothems have recorded the rapid recovery of the soil-ecosystem after a snowball Earth during cap dolostone rebound and karstic dissolution, which is key geological evidence for the 'green' Earth model.

The karstic dissolution surface may have been widely distributed on a global scale at early Ediacaran, implying that the coincident silicified calcareous paleo-speleothems are also global distributed. The silicification preservation process has destroyed some original geochemical information such as carbon/oxygen isotopes, but the plentiful organic-rich laminae are preserved. Thus, the bio-markers in these organic-rich laminae are expected to further document the evolution of soil-ecosystem.

Acknowledgements

This research was supported by the National Nature Science Fund of China (41802027, 41873058), Natural Science and Technology Fund of Guizhou Province, China [JZ(2015)2009], and the incentive subsidy funds from the Guizhou Education University in 2019 for projects of the Ministry of Science and Technology and the National Natural Science Fund of China: Study on paleo-karst structure preserved in cap dolostone of Doushantuo Formation in South China. We thank Ke Pang and Chuanming Zhou for helpful discussions and Joshua Musir for English correction.

Author Contributions

T.L., G.Z., and T.G. designed the research. T.L., G.Z., and T.G. collected the samples. G.Z and T.G. conducted experiments. G.Z., T.G., and T.L. developed the interpretation and prepared the manuscript with contributions from M.Z.

Methods

Three sheet-crack samples (14XFH-1, 14XFH-3 and 14XFH-5) from Xiaofenghe section (N30°48′54″, E111°03′20″), Hubei Provinces, three sheet-crack samples (14DPc1-1, 14DPc1-2 and 14DPc1-3) from Daping section (N28°59′01″, E110°27′42″), Hunan Provinces, four sheet-crack samples (16WH-1, 16WH-2, 16WH-3 and 16WH-

4) from Wenghui section (N27°49′55″, E109°01′32″) , Guizhou Provinces and four samples (18BDS-2, 18BDS-4, 18BDS-7 and 18BDS-9) from Beidoushan section (N27°01′40″, E107°23′22″), Guizhou Provinces were collected from the cap dolostone of the Doushantuo Formation in South China. Petrographic slices (100 μm and 200 μm in thickness) and polished slabs of the sheet-crack samples were cut both perpendicular and horizontal to bedding plane and investigated under transmitted light microscopy (TLM), reflected light microscopy (RLM) and fluorescent light microscopy (FLM).

Reference

1 Kennedy, M., Droser, M., Mayer, L. M., Pevear, D. & Mrofka, D. Late Precambrian oxygenation; inception of the clay mineral factory. *Science* **311**, 1446-1449 (2006).

2 Knauth, L. P. & Kennedy, M. J. The late Precambrian greening of the Earth. *Nature* **460**, 728 (2009).

3 Kump, L. R. Hypothesized link between Neoproterozoic greening of the land surface and the establishment of an oxygen-rich atmosphere. *Proceedings of the National Academy of Sciences* **111**, 14062-14065 (2014).

4 Condon, D. *et al.* U-Pb ages from the neoproterozoic Doushantuo Formation, China. *Science* **308**, 95-98, doi:10.1126/science.1107765 (2005).

5 Zhou, C., Yuan, X., Xiao, S., Chen, Z. & Hua, H. Ediacaran integrative stratigraphy and timescale of China. *Science China Earth Sciences* **62**, 7-24, doi:10.1007/s11430-017-9216-2 (2019).

6 Baker, A., Barnes, W. L. & Smart, P. L. Speleothern luminescence intensity and spectral characteristics: Signal calibration and a record of palaeovegetation change. *Chemical Geology* **130**, 65-76, doi:https://doi.org/10.1016/0009-2541(96)00003-4 (1996).

7 Frisia, S. & Borsato, A. in *Developments in Sedimentology* Vol. 61 (eds A. M. Alonso-Zarza & L. H. Tanner) 269-318 (Elsevier, 2010).

8 Dorr, H. & Munnich, K. O. Annual Variations of the 14C Content of Soil CO2. *Radiocarbon* **28**, 338-345 (1986).

9 Amodio, S., Barattolo, F. & Riding, R. Early Cretaceous dendritic shrub-like fabric in karstified peritidal carbonates from southern Italy. *Sedimentary Geology* **373**, 134-146, doi:10.1016/j.sedgeo.2018.06.001 (2018).

10 Qing, H. & Nimegeers, A. R. Lithofacies and depositional history of Midale carbonate-evaporite cycles in a Mississippian ramp setting, Steelman-Bienfait area, southeastern Saskatchewan, Canada. *Bulletin of Canadian Petroleum Geology* **56**, 209-234, doi:10.2113/gscpgbull.56.3.209 (2008).

11 Freytet, P. & Verrecchia, E. P. Lacustrine and palustrine carbonate petrography: an overview. *Journal of Paleolimnology* **27**, 221-237, doi:10.1023/a:1014263722766 (2002).

12 Alvaro, J. J. & Clausen, S. Microbial crusts as indicators of stratigraphic diastems in the Cambrian Breche a Micmacca, Atlas Mountains of Morocco. *Sedimentary Geology* **185**, 255-265,

doi:10.1016/j.sedgeo.2005.12.025 (2006).

13 Zhou, C., Bao, H., Peng, Y. & Yuan, X. Timing the deposition of 17O-depleted barite at the aftermath of Nantuo glacial meltdown in South China. *Geology* **38**, 903-906 (2010).

14 Hoffman, P. F. & Macdonald, F. A. Sheet-crack cements and early regression in Marinoan (635 Ma) cap dolostones: Regional benchmarks of vanishing ice-sheets? *Earth and Planetary Science Letters* **300**, 374-384, doi:10.1016/j.epsl.2010.10.027 (2010).

15 Allen, P. A. & Hoffman, P. F. Extreme winds and waves in the aftermath of a Neoproterozoic glaciation. *Nature* **433**, 123, doi:10.1038/nature03176 (2005).

16 Jiang, G., Kennedy, M. J., Christie-Blick, N., Wu, H. & Zhang, S. Stratigraphy, sedimentary structures, and textures of the late Neoproterozoic Doushantuo cap carbonate in South China. *Journal of Sedimentary Research* **76**, 978-995 (2006).

17 Zhou, C., Lang, X., Huyskens, M. H., Yin, Q.-Z. & Xiao, S. Calibrating the terminations of Cryogenian global glaciations. *Geology* **47**, 251-254, doi:10.1130/g45719.1 (2019).

18 Condon, D. *et al.* U-Pb Ages from the Neoproterozoic Doushantuo Formation, China. *Science* **308**, 95-98 (2005).

19 Zhou, G., Luo, T., Zhou, M., Xing, L. & Gan, T. A ubiquitous hydrothermal episode recorded in the sheet-crack cements of a Marinoan cap dolostone of South China: Implication for the origin of the extremely C-13-depleted calcite cement. *Journal of Asian Earth Sciences* **134**, 63-71, doi:10.1016/j.jseaes.2016.11.007 (2017).

20 Fairchild, I. J. & Baker, A. *Speleothem science: from process to past environments*. Vol. 3 (John Wiley & Sons, 2012).

21 Gams, I. Contribution to morphometrics of stalagmite. *Proceedings of the 8th International Congress of Speleology* **8**, 276-278 (1981).

22 Tan, M. *et al.* Applications of stalagmite laminae to paleoclimate reconstructions: Comparison with dendrochronology/climatology. *Quaternary Science Reviews* **25**, 2103-2117, doi:https://doi.org/10.1016/j.quascirev.2006.01.034 (2006).

23 Baker, A., Smart, P. L., Edwards, R. L. & Richards, D. A. ANNUAL GROWTH BANDING IN A CAVE STALAGMITE. *Nature* **364**, 518-520, doi:10.1038/364518a0 (1993).

24 Tan, L. *et al.* Quantitative temperature reconstruction based on growth rate of annually-layered stalagmite: a case study from central China. *Quaternary Science Reviews* **72**, 137-145, doi:10.1016/j.quascirev.2013.04.022 (2013).

25 Railsback, L. B. *et al.* The timing, two-pulsed nature, and variable climatic expression of the 4.2 ka event: A review and new high-resolution stalagmite data from Namibia. *Quaternary Science Reviews* **186**, 78-90, doi:https://doi.org/10.1016/j.quascirev.2018.02.015 (2018).

26 Dreybrodt, W. & Romanov, D. REGULAR STALAGMITES: THE THEORY BEHIND THEIR SHAPE. *Acta Carsologica* **37**, 175-184 (2008).

27 Tan, L. *et al.* Quantitative temperature reconstruction based on growth rate of annually-layered stalagmite: A case study from central China. *Quaternary Science Reviews* **72**, 137-145 (2013).

28 Baker, A., Smart, P. L., Edwards, R. L. & Richards, D. A. Annual growth banding in a cave stalagmite. *Nature* **364**, 518-520 (1993).

29 Baker, A., Proctor, C. J. & Barnes, W. L. Stalagmite lamina doublets: a 1000 year record of extreme winters in NW Scotland. *International Journal of Climatology* **22** (2002).

30 Wang, X. *et al.* PRELIMINARY ANALYSES BY SIMS ON TRACE COMPONENTS OF STALAGMITE MICROLAYERS AND THEIR CLIMATE SIGNIFICANCE. *Quaternaryences* **19**, 59-66,97-98 (1999).

31 Brook, G. A., Rafter, M. A., Railsback, L. B., Sheen, S. W. & Lundberg, J. A high-resolution proxy record of rainfall and ENSO since AD 1550 from layering in stalagmites from Anjohibe Cave, Madagascar. *Holocene* **9**, 695-705, doi:10.1191/095968399677907790 (1999).

32 Aubrecht, R., Brewercarias, C., Smida, B., Audy, M. & Kovacik, Ľ. Anatomy of biologically mediated opal speleothems in the World's largest sandstone cave: Cueva Charles Brewer, Chimantá Plateau, Venezuela. *Sedimentary Geology* **203**, 181-195 (2008).

33 R, C., T, T. & Y, X. *Research on Sinian Strata with ore deposits in the Yangzi (Yangtze) region, China*. (1989).

34 Wheeler, W. H. & Textoris, D. A. Triassic Limestone and Chert of Playa Origin in North Carolina. *Journal of Sedimentary Research* **48**, 765-776 (1978).

35 Skotnicki, S. J. & Knauth, L. P. The Middle Proterozoic Mescal Paleokarst, Central Arizona, U.S.A.: Karst Development, Silicification, and Cave Deposits. *Journal of Sedimentary Research* **77**, 1046-1062 (2007).

36 Cui, Y. *et al.* Germanium/silica ratio and rare earth element composition of silica-filling in sheet cracks of the Doushantuo cap carbonates, South China: Constraining hydrothermal activity during the Marinoan snowball Earth glaciation. *Precambrian Research*, 105407, doi:https://doi.org/10.1016/j.precamres.2019.105407 (2019).

37 Blyth, A. J. *et al.* Molecular organic matter in speleothems and its potential as an environmental proxy. *Quaternary Science Reviews* **27**, 905-921 (2008).

38 Kaufmann, G. Stalagmite growth and palaeo-climate: the numerical perspective. *Earth and Planetary Science Letters* **214**, 251-266 (2003).

39 Bosak;, P., Ford;, D. C., Glazek;, J. & Horacek, I. (Academia, Publishing House of the Czechoslovak Academy of Sciences, Prague, Czechoslovakia, 1989).

40 Semeniuk, V., Percival, I. G. & Brocx, M. Subaerial disconformities, microkarst and paleosols in Ordovician limestones at Bowan Park and Cliefden Caves, New South Wales, and their geoheritage significance. *Australian Journal of Earth Sciences* **66**, 891-906, doi:10.1080/08120099.2019.1577297 (2019).

41 Kerans, C. & Donaldson, J. A. *Proterozoic Paleokarst Profile, Dismal Lakes Group, N.W.T., Canada 1*. (1988).

42 Ding, Y. *et al.* Cavity-filling dolomite speleothems and submarine cements in the Ediacaran Dengying microbialites, South China: Responses to high-frequency sea-level fluctuations in an 'aragonite-dolomite sea'. *Sedimentology*, doi:10.1111/sed.12605 (2019).

Figure Legends

Figure 1 | Polished slab and micrographs of stalactite from Beidoushan section. a, Polished slab shows stalactites in a sheet-crack scanning by a HP ScanJet, the white solid rectangle highlights a column (connective bodies of stalactite and stalagmite), white dotted rectangles highlight conjuction stalactites, the yellow arrow denotes a single complete stalactite with "soda straw" drip channel. **b**, Petrogrphic slice shows transverse and vertical sections of stalactite under TLM (transmission light microscope), the white and red arrows denote the vertical and transverse sections of "soda straw" drip channel, respectively. **c**, Enlarged view of the stalactite vertical section in **b** (rectangle) under FLM (fluorescent light microscope), the white arrow denotes the vertical section of "soda straw" drip channel. **d**, Enlarged view of stalactite transverse in **b** (rectangle) under FLM, red arrows denote the transverse of "soda straw" drip channel.

Figure 2 | Polished slabs and micrographs of stalagmite, stalactite and coating from Wenghui section. a, Polished slab showing stalagmite, stalactite and coating in a sheet-crack, white dotted lines highlight the coating areas in the sheet-crack, white arrows denote stalactites, yellow arrows denote stalagmites. **b**, Petrographic slice shows a vertical section of stalagmite and coating under RLM, white dotted lines highlight the coating areas. **c**, Enlarged view of coating vertical section shows the organic-rich laminae in **b** (rectangle) under FLM. **d**, Petrographic slice shows stalagmite and stalactite transverses under TLM, red arrows and yellow arrows denote a single "soda straw" drip channel and the aggregation of "soda straw" drip channel, respectively. **e**, Enlarged view of a stalactite vertical section in **d** (rectangle) under FLM, showing the organic-rich laminae and "soda straw" drip channel. **f**, Enlarged view of a stalagmite transverse section in **d** (rectangle) under FLM, showing the organic laminae but lack of "soda straw" drip channel.

Figure 3 | Polished slab, hand specimen and micrographs of coatings and a special stalactite. a, Polished slab shows coatings in a sheet-crack, white arrows denote the coating of a dolostone breccia. **b**, Hand specimen shows a coating lining in a sheet-crack, white dotted line highlights the coating boundary, black and red arrow denote botryoidal and mold structure of the coating. **c**, Petrographic slice shows a coating with a vermiform-like helictite under FLM. **d**, Enlarged view of the helictite in **c** (rectangle) under SEM (scanning electron microscope). **e**, Petrographic slice shows a partly silicified organic-rich calcareous coating under TLM. **f**, Enlarged view of the coating in **e** (rectangle) under SEM, showing the silicified calcareous coating, white arrows highlight the siliceous cements. **g**, Enlarged view of the coating in **e** (rectangle) under FLM, showing the organic-rich laminae. **h**, Petrographic slice shows a silicified stalactite under TLM, white arrows highlight the residual calcite laminae. **a, c** and **d** from Beidoushan section, **b** from Zhangcunping section, **e-g** from Daping section, **h** from Xiaofenghe section.

Fig. 1

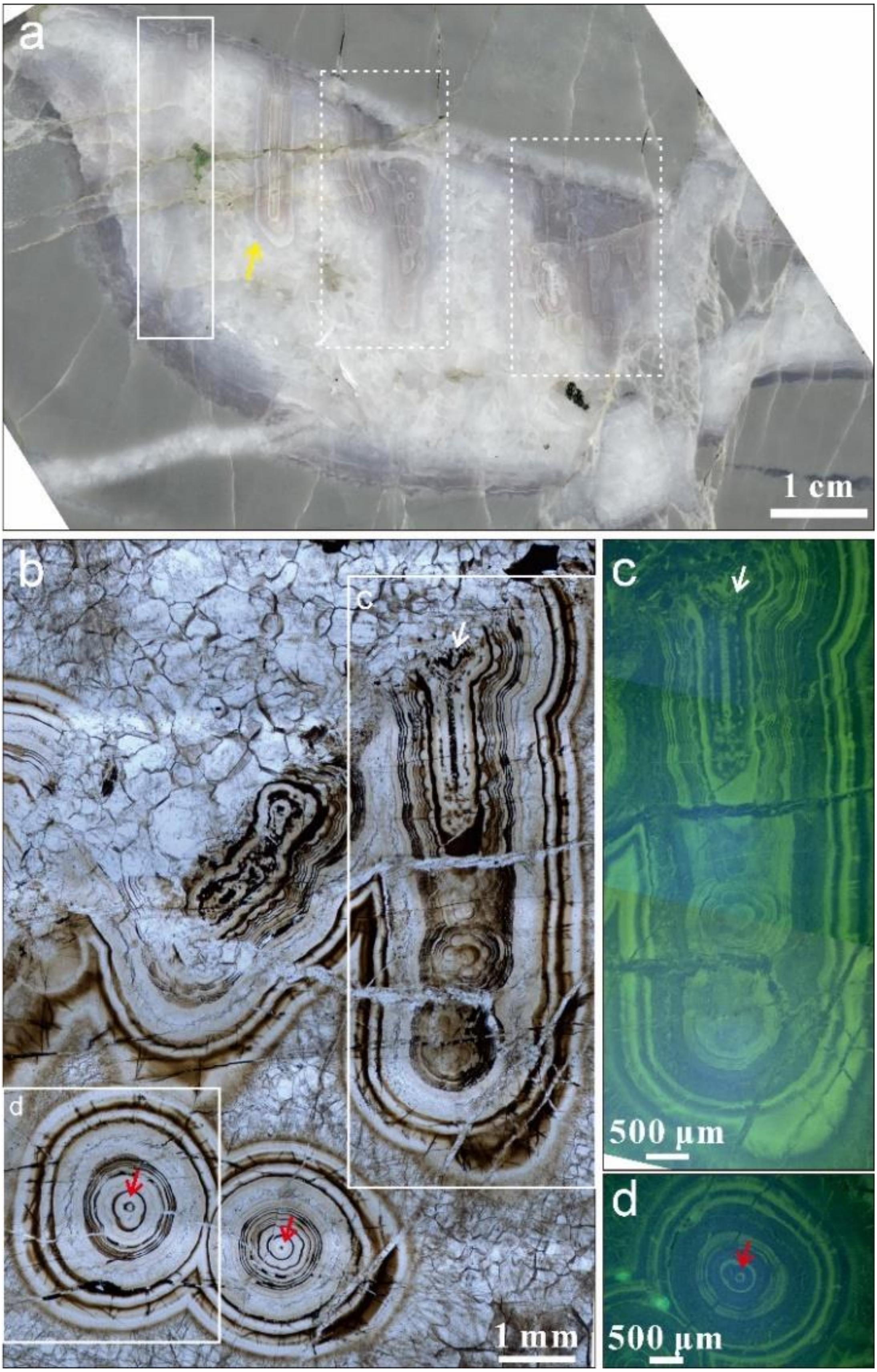

406

Fig. 2

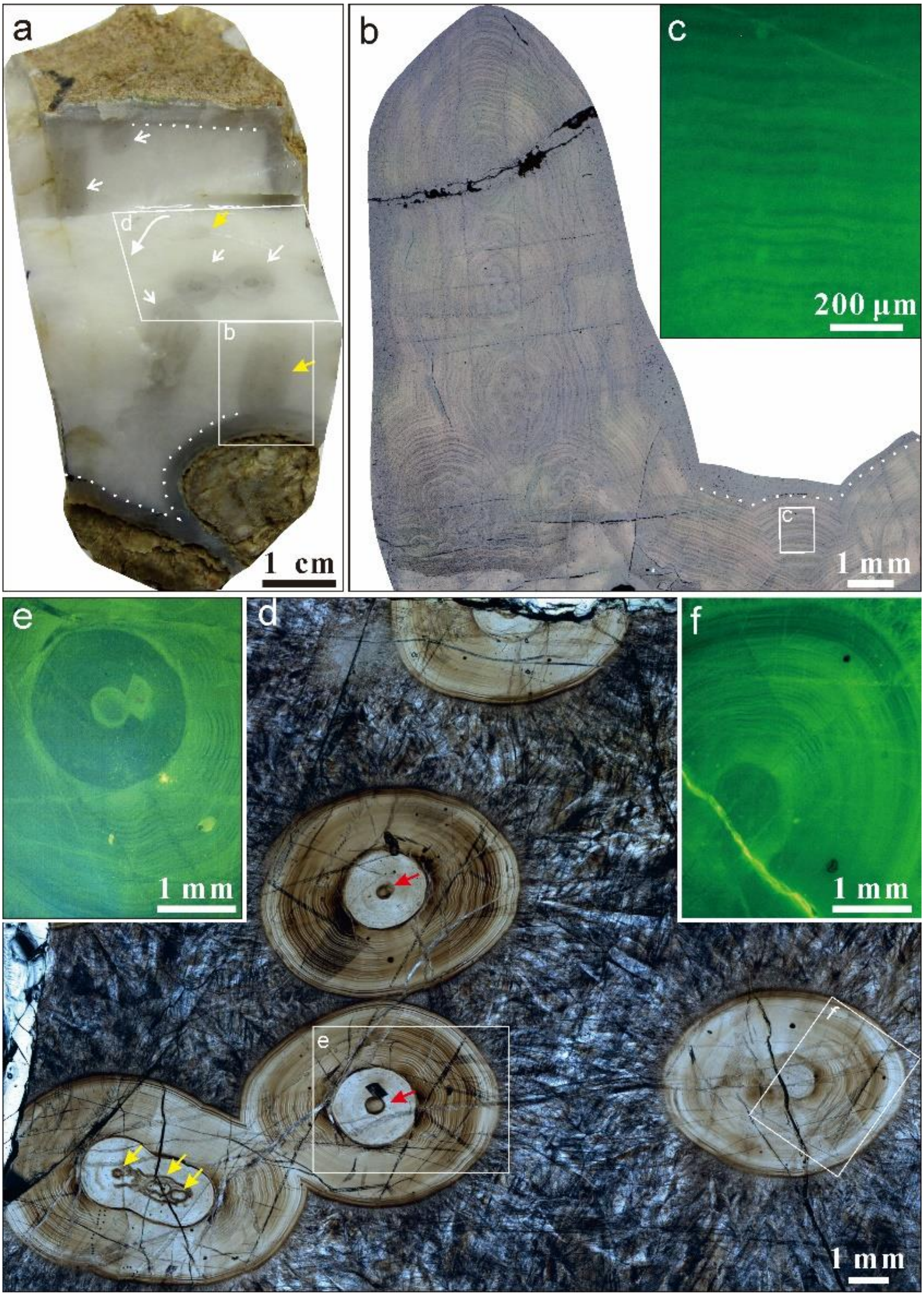

407

408

409 **Fig. 3**

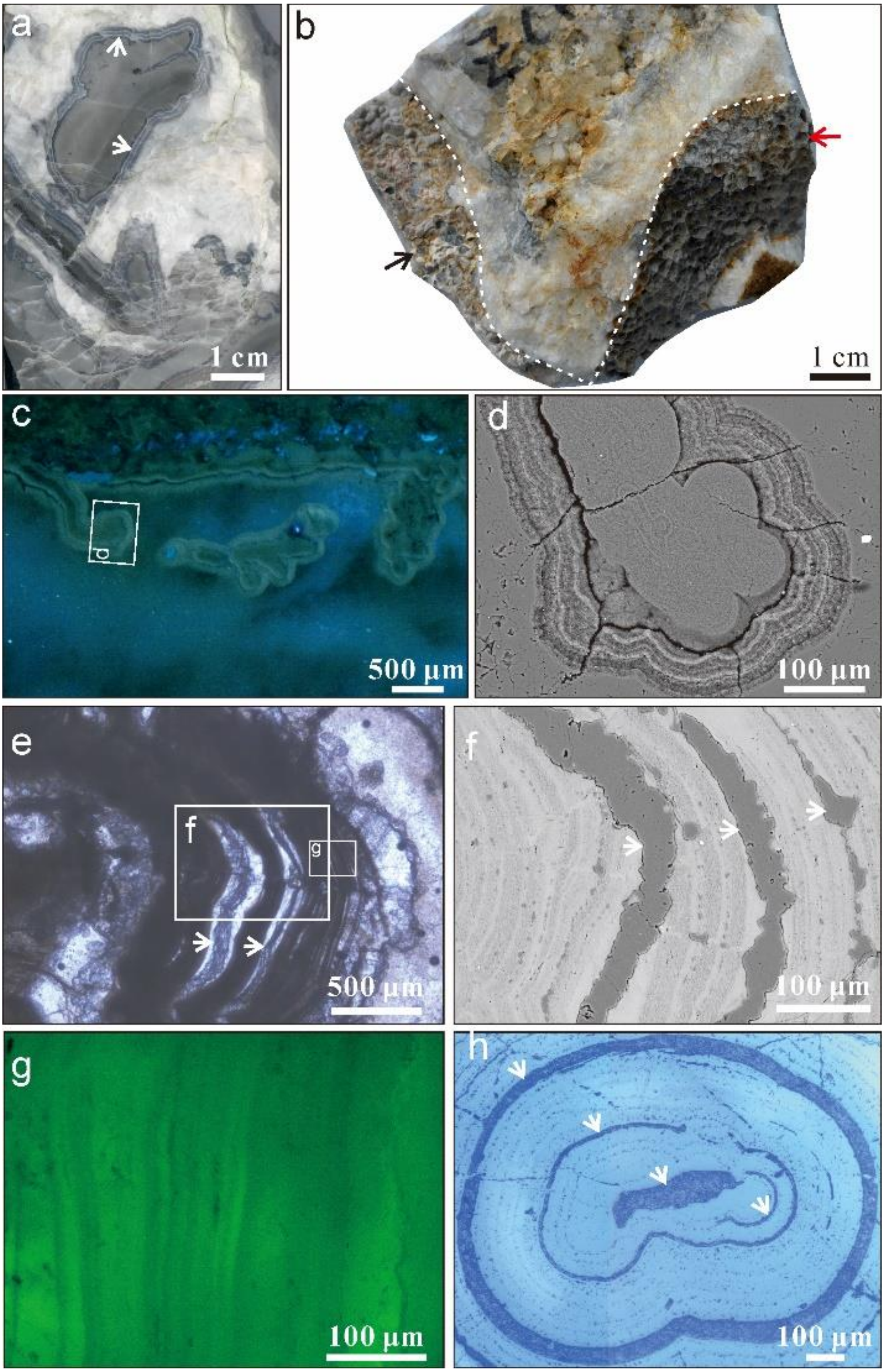

410